AGU PUBLICATIONS

Geophysical Research Letters

RESEARCH LETTER
10.1002/2016GL069485

Key Points:
- Modern satellite sea surface temperature data clarify tidal mixing signatures in Indonesian seas
- Spring-neap SST signals are mostly localized to straits and sills; not evident in the deep Banda Sea
- Major straits of the Lesser Sunda Island chain display strong, complex mixing signatures

Correspondence to:
R. D. Ray,
richard.ray@nasa.gov

Citation:
Ray, R. D., and R. D. Susanto (2016), Tidal mixing signatures in the Indonesian seas from high-resolution sea surface temperature data, *Geophys. Res. Lett.*, *43*, doi:10.1002/2016GL069485.

Received 18 MAR 2016
Accepted 18 JUL 2016
Accepted article online 23 JUL 2016

Tidal mixing signatures in the Indonesian seas from high-resolution sea surface temperature data

Richard D. Ray[1] and R. Dwi Susanto[2,3]

[1]NASA Goddard Space Flight Center, Greenbelt, Maryland, USA, [2]Department of Atmospheric and Oceanic Science, University of Maryland, College Park, Maryland, USA, [3]Center for Oceanography and Marine Technology, Surya University, Tangerang, Indonesia

Abstract The presence of significant tidal mixing in the Indonesian seas is well established from both observations and numerical modeling. One indicator is a clear spring-neap cycle in satellite sea surface temperature (SST) measurements, as first shown by Ffield and Gordon. Their early results are here updated with SST data of considerably higher spatial and temporal resolution. The largest fortnightly signals are found to be localized to relatively small straits, channels, and sills, while the deep basin of the Banda Sea displays little significant signal. A broader region of somewhat enhanced signal surrounds the Seram Sea. The high resolution of the modern SST data is especially critical for mapping the complex fortnightly signals that arise in, and especially south of, the major straits of the Lesser Sunda Island chain.

1. Introduction

Two decades ago *Ffield and Gordon* [1996] (hereafter FG96) provided some of the first direct evidence of strong tidal mixing in the Indonesian seas when they detected a pronounced spring-neap tidal cycle in satellite sea surface temperature (SST) data. Since then the evidence for tidal mixing in this region has grown only stronger [*Sprintall et al.*, 2003; *Hatayama*, 2004; *Koch-Larrouy et al.*, 2007, 2010, 2015; *Nagai and Hibiya*, 2015]. The importance of tidal mixing to the transformation of Pacific and Indonesian throughflow water and to the climate system in general was recently reviewed by *Sprintall et al.* [2014].

As FG96 recognized, if tidal mixing is indeed acting to perturb observed SST, one characteristic signature—at least in a location of predominantly semidiurnal tides—could be a signal at the spring-neap cycle, with period 14.77 days. Stronger spring tide currents, occurring when the principal M_2 and S_2 constituents are in phase, act to lower SST as colder subsurface water is mixed upward. Depending on the tidal regime, other frequencies could also appear (see section 2), but here we focus on the main spring-neap cycle which is the period most typically expected. Indeed, fortnightly SST signals, often associated with tidal fronts, are not uncommon features in many gulfs and shallow seas [e.g., *Paden et al.*, 1991; *Bisagni and Sano*, 1993; *Souza and Pineda*, 2001; *Martínez Díaz de León et al.*, 2013].

The quality of the SST data available to Ffield and Gordon was very much inferior to SST data now widely available. The temporal sampling of their SST data was weekly and thus barely adequate for studying a fortnightly signal; the spatial sampling was so crude that the entire island of Borneo (the world's third-largest island) was indistinguishable from open sea. In contrast, high-resolution modern data—high in both space and time—now allows us to obtain a much clearer picture of the mixing signatures, as we show here.

Some of the most useful of the modern SST data are those produced under the auspices of the Group for High-Resolution Sea Surface Temperature (GHRSST) [*Donlon et al.*, 2009]. Their goal has been to produce high-level SST products that merge data from different satellites and different sensors in an optimal way. Measurements with infrared (IR) sensors, from systems such as the Advanced Very High Resolution Radiometers (AVHRR), form the backbone of a multidecadal time series. The IR measurements provide high spatial resolutions of order 1–2 km, but they are obstructed by clouds, which can be problematic in the Indonesia region. Microwave sensors provide data in nearly all weather conditions but at considerably coarser spatial resolution, of order 25–50 km [*Wentz et al.*, 2000], and they require a mask of 50–75 km around land, depending on the sensor specifics, owing to the large microwave footprint and the possible contamination when land

Table 1. Expected Periods in SST From Tidal Mixing

Interacting Tides	Equivalent Linear Tide	Argument[a] $\Theta(t)$	Frequency $d\Theta/dt$ (°/h)	Period (Days)
K_1-O_1	Mf	$2s$	1.09803	13.66
S_2-M_2	MSf	$2s - 2h$	1.01590	14.77
M_2-N_2	Mm	$s - p$	0.54438	27.55

[a]The tidal argument variables are as follows [*Doodson and Warburg*, 1941; *Pugh and Woodworth*, 2014]: s, mean longitude of the Moon; h, mean longitude of the Sun; and p, mean longitude of lunar perigee.

falls within the antenna side lobes [e.g., *Chelton and Wentz*, 2005]. The GHRSST products aim to achieve the best combination of these different systems.

2. Tidal Frequencies in SST

We assume, as did FG96, that the change in ocean temperature induced by tidal mixing depends on the square of the tidal current velocities. This follows from simple models of turbulent mixing parameterized in terms of a diffusivity K_v that is subjected to tidal perturbations. K_v depends [e.g., *Osborn*, 1980] linearly on a turbulent dissipation rate linked to the available kinetic energy in the tides themselves, which scales with the square of current velocities.

Given two constituents, $A_1 \cos \omega_1 t + A_2 \cos \omega_2 t$, squaring generates oscillatory motion at a lower frequency $|\omega_2 - \omega_1|$ (as well as at higher frequencies like $(\omega_1 + \omega_2)$, which need not concern us). This is quite similar to the generation of nonlinear compound tides in shallow water, although in that case the new frequencies arise from nonlinear terms in the tidal equations of motion rather than nonlinear terms in the physics of mixing.

Table 1 presents a list of the low-frequency (weekly and longer) SST signals that one might expect to be generated by the largest diurnal and semidiurnal tidal constituents. The table shows for each generated frequency the short-period tides that are interacting, and it also lists the linear long-period constituent that may exist at that same frequency. (The linear constituents are shown primarily because they give us convenient labels; the long-period constituents themselves, with very small current velocities, are too weak to be involved in the physics.) In most parts of the world, the 14.77 day signal should be most conspicuous, if indeed any are. In places like the Gulf of Maine, N_2 is larger than S_2, which leads to a "perigean cycle" of one anomalistic month or 27.55 days. Where diurnal tides dominate (e.g., in parts of the South China Sea; also Okhotsk Sea [*Rogachev et al.*, 2001]), the near-fortnightly signal will be 13.66 days and not 14.77 days. The two signals are separable in about half a year.

Not included in Table 1 are tidal frequencies interacting with their neighboring 18.6 year nodal frequencies, which would give rise to 18.6 year oscillations in SST. To the extent that this can occur, it would involve mainly the diurnal O_1 and K_1 constituents [*Ray*, 2007]. There have been a handful of credible reports of the nodal cycle in climate variables [e.g., *Osafune and Yasuda*, 2006] (and many more reports not so credible). Detection requires SST time series significantly longer than those employed here.

3. SST Data

During the course of this work we have used a number of different SST products. For debugging purposes we have even used the Climate Analysis Center (CAC) version 1 data [*Reynolds and Marsico*, 1993] used by FG96. In this paper we concentrate on results obtained with the Multiscale Ultrahigh Resolution SST (MUR-SST) product which is produced at the Jet Propulsion Laboratory [*JPL MUR MEaSUREs Project*, 2010; *Chin et al.*, 2013]. The MUR-SST product, based on both IR and microwave measurements, merges data from a large number of satellites by an objective interpolation technique based on a wavelet decomposition method [*Chin et al.*, 1998]. MUR-SST data are available from June 2002 to present.

The MUR-SST data are released on a uniform latitude-longitude grid with sampling of 0.01° or approximately 1 km. As emphasized by *Reynolds and Chelton* [2010] in their comparison of a number of different SST products, grid resolution is in no sense equivalent to actual spatial resolution. The MUR-SST documentation presents evidence that its inherent resolution is of order 10 km and is better than that available from most other GHRSST products. We find below that some of the SST signatures of most interest do benefit from this high spatial resolution.

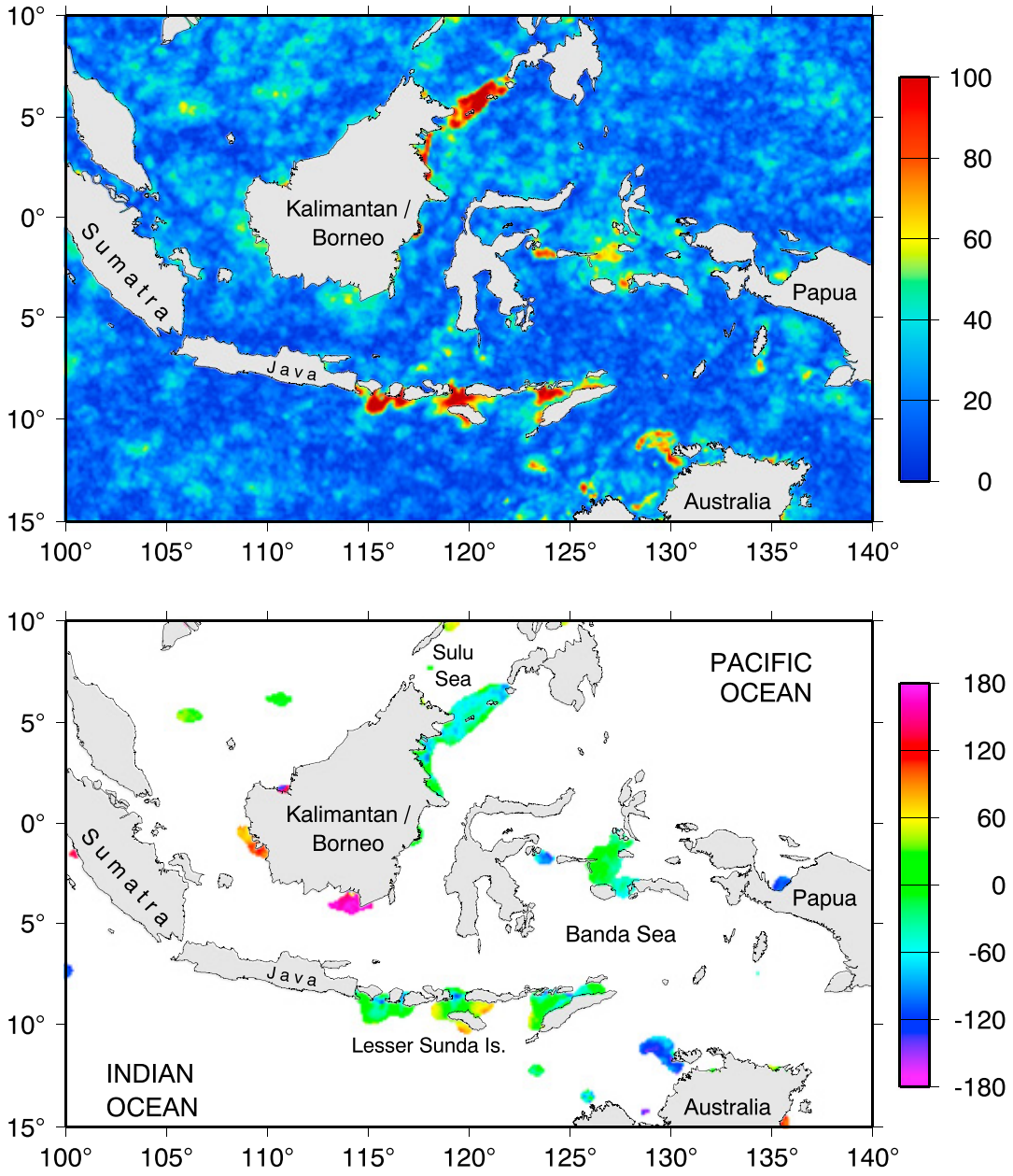

Figure 1. Estimates of (top) amplitude (in millikelvin) and (bottom) Greenwich phase lag (in degrees) of the spring-neap (MSf) tidal component in sea surface temperature, extracted from over 12 years of MUR-SST data. Phases are shown only in locations where the amplitude exceeds twice its standard error.

Donlon et al. [2007] give a useful overview of the accuracies of individual SST measurements, generally ranging from 0.2°C to 1°C depending on sensor type and other factors (also *Chin et al.* [2013]). As with any tidal analysis, what concerns us here is the measurement noise—and also the nontidal variability—that falls precisely at the tidal frequency of interest. As shown below, in the near-fortnightly band of the MUR-SST data this noise appears to be roughly of order 20 mK (0.02°C).

4. Results

Figure 1 shows the main results of extracting the 14.77 day MSf amplitudes A and phase lags G from the 12.5 year MUR-SST time series (June 2002 through November 2014). The MSf wave is parameterized as

$$\mathrm{SST} = A\cos(\Theta(t) - G) \tag{1}$$

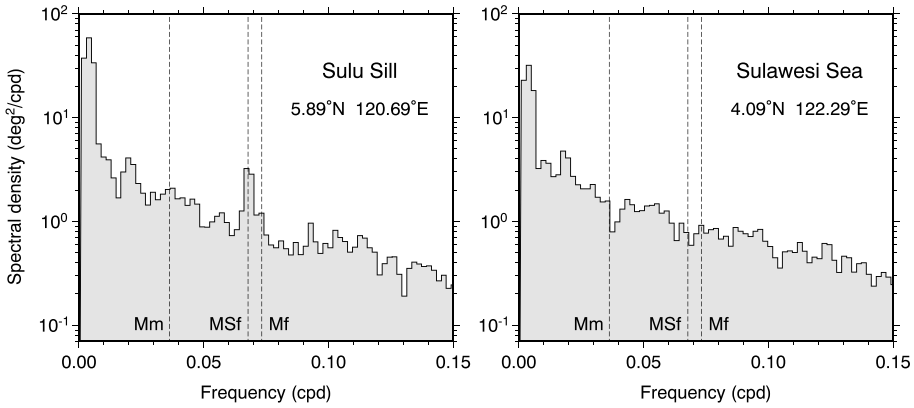

Figure 2. SST spectra based on 12 years of daily MUR-SST data at (left) a location along the southern boundary of the Sulu Sea where the MSf peak is pronounced and (right) in the interior of the Sulawesi Sea where the peak is missing. Labeled vertical dashed lines mark frequencies of the three long-period tides of Table 1; the spectral peaks at far left occur at the annual and semiannual frequencies. Near MSf the background level is clearly below 1 K^2/cpd. With a frequency resolution of $(12\ \text{years})^{-1}$ this background thus corresponds to a noise level somewhat below 0.02 K.

where the argument $\Theta(t)$ is given by [*Doodson and Warburg*, 1941, Table 7.1]

$$\Theta(t) = 2s(t) - 2h(t) \tag{2}$$

where $s(t)$ and $h(t)$ are the mean longitudes of the Moon and Sun, respectively, reckoned as usual from the vernal equinox. The strongest signals in Figure 1 have amplitudes of order 100 mK (0.1°C), and all are localized to relatively narrow channels, straits, and sills.

We have determined standard errors for the tide estimates in two ways: (a) from the diagonals of the least squares covariance matrix after scaling by the residual noise variance, the latter estimated from the spectral densities in the neighborhood of the tidal frequencies, and (b) by estimating amplitudes of several "false" tides, at nontidal frequencies in the vicinity the MSf and Mf lines. The two approaches are reasonably consistent. Examination of the errors at a number of locations across the region yielded a median standard error from (a) of 22 mK and from (b) 18 mK. Figure 1 displays phases at only those locations where the estimated MSf amplitudes exceed twice the standard error.

The largest signals in Figure 1 are indeed robust and well determined. For example, the SST spectrum for one of these high-amplitude points on the Sulu Sea sill is shown in Figure 2. The MSf peak is well above background and is fairly sharp. There is also suggestion of a subtler enhancement of SST energy across a range of near-fortnightly frequencies, starting somewhat below the MSf frequency and including Mf, but the MSf peak itself sits well above this "cusp." At this location the estimated MSf amplitude is 119±22 mK and the phase lag is −70°±11°.

Nearly all the large-amplitude spots of Figure 1 occur in regions displaying very strong M_2 current velocities, some exceeding 100 cm s^{-1} [*Ray et al.*, 2005, Figure 4]. Some of the highest amplitudes are also places that experience intense M_2 barotropic energy fluxes, especially through the major straits of the Lesser Sunda Island chain between Bali and Timor where the semidiurnal tide propagates into the Indonesian region from the Indian Ocean. In several of these straits, *Sprintall et al.* [2003] also observed strong fortnightly signals in in situ temperature measurements. The southern sill of the Sulu Sea, with very strong velocities although only moderate energy fluxes [*Ray et al.*, 2005, Figure 5], is a well-known source for large internal solitons [*Apel et al.*, 1985; *Tessler et al.*, 2012]. In light of all these facts, it is reasonable to conclude, as did FG96, that the MSf signals of Figure 1 reflect, in one way or another, the presence of tidal mixing. Whether other mechanisms are also involved (e.g., upwelling of deeper and tidally mixed water) requires further investigation. Possible advection of mixing signatures appears evident in some locations (see below).

All the high-amplitude spots of Figure 1 also correspond to locations where the 3-D tidal model of *Nagai and Hibiya* [2015, Figure 9] predicts significant dissipation of baroclinic energy. On the other hand, the reverse is not true: the Nagai-Hibiya model predicts significant dissipation in some regions where we find very little MSf signal. A notable example is along the Sangihe Island chain between Sulawesi and the Philippines, following

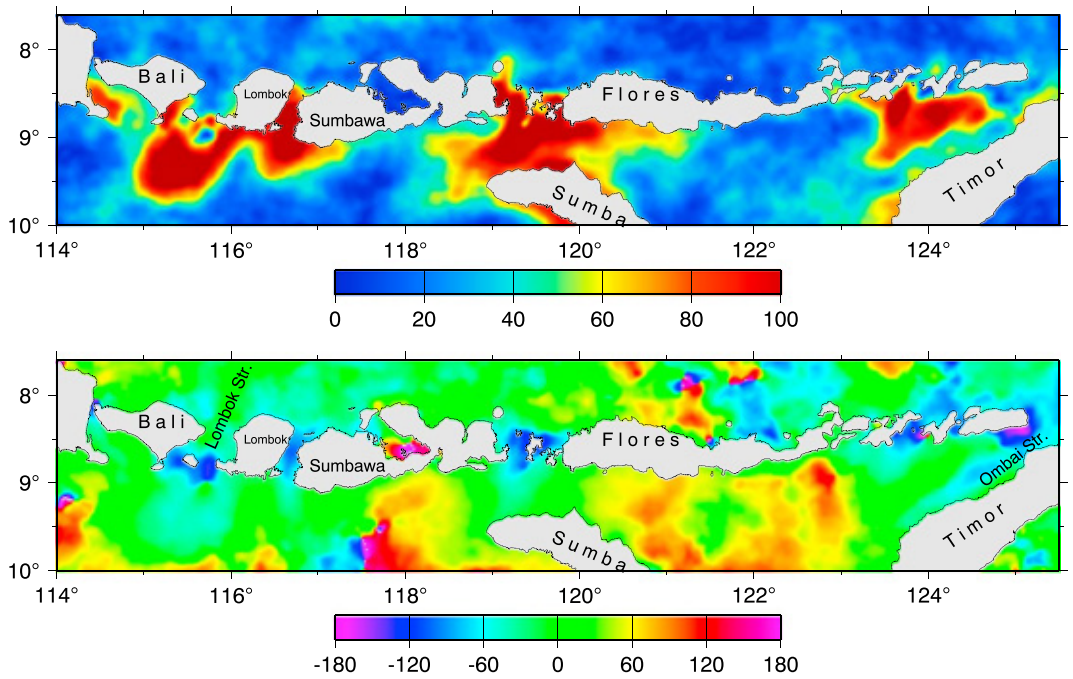

Figure 3. Estimates of (top) amplitude in millikelvin and (bottom) Greenwich phase lag in degrees, of the spring-neap (MSf) tidal component in sea surface temperature, focusing on the southern part of the Lesser Sunda Island chain. The regions of largest amplitudes all have phase lags of about −50°, but the phase lags within the major straits themselves are closer to −120° or about 3 days earlier.

approximately the 125°E meridian, where the model baroclinic dissipation is high. If the Nagai-Hibiya simulation is realistic, then some possible explanations for a weak SST signal are: (i) tidal mixing is localized near the bottom and does not affect the surface; (ii) the location is characterized by an especially low mixing efficiency; (iii) the S_2 constituent (or potentially even the M_2 constituent) is so weak that the tidal mixing is no longer modulated in time by the spring-neap cycle. Thus, while a high MSf amplitude indicates mixing associated in some manner with tides, a low amplitude does not rule it out.

The localized nature of the fortnightly SST signals in Figure 1 is in sharp contrast to the broad-scale regional signals that FG96 found with the older CAC SST product. In their case the regions with high MSf amplitudes included a wide swath from the Java Sea south of Sulawesi running eastward across nearly the whole of the Banda Sea. It now seems likely that that broad-scale, regional signal was an artifact, a large-scale "smearing" of shorter-scale signals, which arose from the large spatial and temporal interpolations used to generate the CAC product.

In light of these differences with FG96, the new results help solve an outstanding puzzle regarding the Banda Sea. It has long been unclear why microstructure measurements in the central Banda Sea by *Alford et al.* [1999] were so inconsistent with the idea of significant tidal mixing at that location. For example, Alford et al. found no fortnightly signal in kinetic energy dissipation, and their estimated diapycnal diffusivity was low, more characteristic of that of the deep, interior ocean. In light of Figure 1, however, the findings by Alford et al. are not so surprising. Their measurements were in a location that shows no significant fortnightly SST signal.

There is, however, a fairly broad region of higher SST amplitudes that is more consistent with FG96 results. This is in the general area of the Seram and Halmahera Seas (between Sulawesi on the west and western New Guinea on the east) where we find moderate amplitudes in the 40–60 mK range. Using a numerical model, *Koch-Larrouy et al.* [2007] show that the South Pacific Water undergoes strong mixing within the Seram/Halmahera Seas prior to entering the Banda Sea; see also *Nagai and Hibiya* [2015, Figure 12a]. Observations from the Indonesian Mixing program [*Koch-Larrouy et al.*, 2015] subsequently confirmed these modeling results. Our amplitudes in this region appear marginally above background noise levels.

The large fortnightly SST signals along the Lesser Sunda Islands are seen in much better detail in Figure 3, where the high spatial resolution of the MUR-SST data can be readily appreciated and indeed seems critical.

The largest amplitudes are seen to appear not within the narrow interisland channels, or at least not exclusively there, but rather to the south. At Lombok Strait, near longitude 115°E, the largest SST amplitudes occur almost 75 km south of the strait sills.

The high resolution provided by the MUR-SST data in this region near Lombok, as well as around the other nearby straits, opens up a unique view into the ocean's interior processes and in particular the mixing processes that SST may reflect. Moreover, Figures 1 and 3 also raise some interesting questions of interpretation that cannot be adequately addressed in this short letter. The large SST amplitudes occurring south of the Sunda Island straits call to mind the SST snapshot shown by *Matthews et al.* [2011, Figure 2] of warm surface water intruding from Lombok Strait out into the deeper Indian Ocean, carried by the strong southward throughflow [*Murray and Arief*, 1988]. The fact that the MSf amplitudes intensify to the south of Lombok Strait (and other straits) may merely reflect the distances over which internal waves propagate before they break. Yet in Lombok Strait, for example, stratification allows internal solitary waves to propagate both northward and southward from the strait [e.g., *Susanto et al.*, 2005], and models of internal wave energy fluxes [*Aiki et al.*, 2011] suggest propagation distances exceeding 100 km in both directions from the strait. So it is not solely internal wave breaking that is key to the large amplitudes south of the strait.

Some additional clues can be extracted from the tidal phase estimates of Figure 3. At those locations where amplitudes exceed about 90 mK, the phases are consistently around −50° (as they also are at the Sulu sill in Figure 1). But within the narrowest parts of the three major straits, the phases tend to be earlier, around −120°. The phase patterns indicate propagation both northward and southward away from the straits, with the southward features growing in amplitude before decaying as they move farther south, as well as somewhat east and west into the deeper ocean. As the amplitudes decay further, even farther south of the island chain, the phases are all around 60° – 90°. So the phase progression from −120° through 0° to 60° represents a "wave" of SST anomalies propagating at least 180° or over a time period of at least half the spring-neap cycle. The clear southward progression from the Sunda Island straits into the deep Indian Ocean suggests advection of tidally oscillating surface temperatures by the strong throughflow.

How do these SST phases correspond to the tidal forcing? The maximum astronomical potential of MSf occurs when the argument $\Theta(t)$ in (2) equals zero, which occurs coincident with spring-tide forcing during either new moon when $s = h$ or full moon when $s = h + 180°$. As FG96 discuss, it is not the potential but rather the resulting spring-tide currents that directly generate mixing signatures. Maximum currents tend to occur somewhat after maximum spring-tide potential, with the delay defined by the somewhat archaic Victorian term, the "age of the tide." The age can be computed from either observations or models of the tide (either elevations or currents), given sufficient horizontal resolution. Here we have used the regional inverse model of *Egbert and Erofeeva* [2002, §5] which is defined on a $\frac{1}{6}°$ grid. Given semidiurnal phases G in degrees, the age T_a is given by

$$T_a = \frac{G(\mathrm{S}_2) - G(\mathrm{M}_2)}{1.0159} \text{ hours} \tag{3}$$

where the denominator is the difference between the S_2 and M_2 frequencies in units of degrees per hour. The computed ages for our region of interest are shown in Figure 4.

Consider first the simpler case of the large SST signature along the Sulu Sea sill, with MSf phase lag of about −70°, which corresponds to a 3 day lead on the potential. The *minimum* SST, which is the sought-for signature of maximum mixing, thus lags the potential by 110° or 4.5 days. Since the age of the semidiurnal tide at this location is about 30 h, or 1.2 days behind the potential, the SST minimum occurs 3.3 days after maximum spring-tide currents.

A lag of 3 days represents about 1/5 the spring-neap cycle. It is of interest to compare this with the lag found in a simple one-dimensional diffusivity model developed by *Garrett* [1979], where mixing is considered to induce small tidal perturbations to diffusivity and the resulting minimum SST is found to lag by about 1/8 the period (or about 2 days for the MSf period). Our observed lag is thus comparable (within 50%) to that predicted by Garrett's one-dimensional model.

The SST signals within the Lesser Sunda Island straits, which appear unlikely to be explained by a one-dimensional model, have MSf phase lags of −120° to −90°, while the age of the semidiurnal tide is between 40 and 50 h or roughly 2 days. Thus, within the straits the minimum SST occurs only about 1 day after

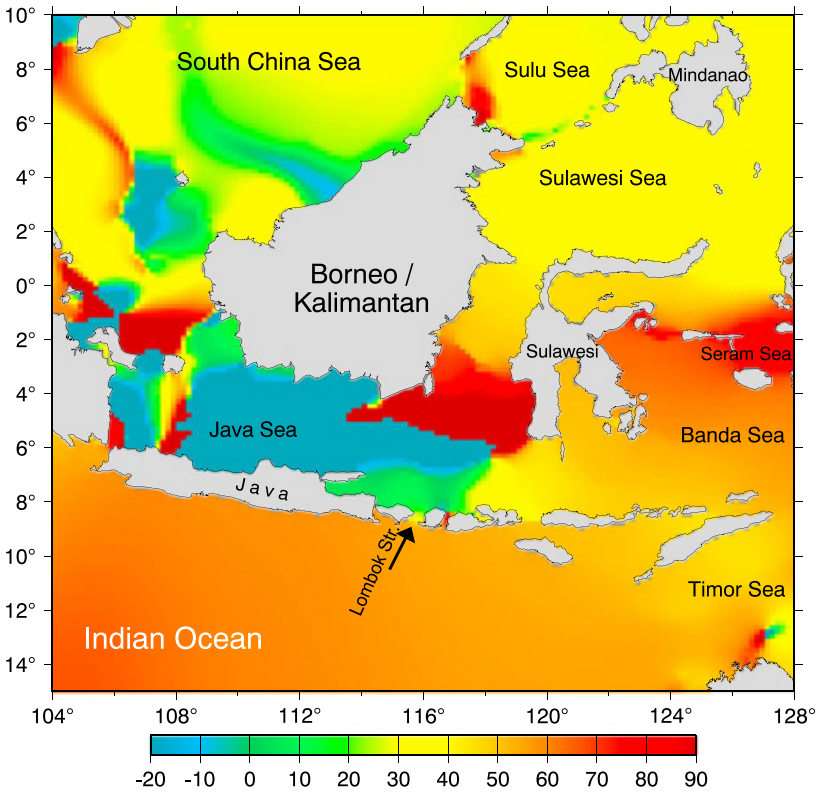

Figure 4. Age of the tide, in hours, based on the M_2 and S_2 inverse solutions of *Egbert and Erofeeva* [2002]. The age is indeterminate in regions of weak M_2 and/or S_2 amplitudes, which is generally the case south and west of Borneo.

maximum spring-tide currents. However, as noted above, the largest SST signatures occur to the south of the straits, with an additional lag of 3 days at those spots where the amplitudes are largest. As the amplitudes grow smaller away from these high spots the phases indicate additional lags over several more days.

5. Discussion

The high-resolution MUR-SST data, with its time series beginning in 2002, gives a picture of the tidal mixing signatures present in the Indonesian seas that is much clearer than the picture obtainable from the early satellite SST data available to FG96 20 years ago. Aside from the broad region surrounding the Seram Sea, where the SST signature is enhanced marginally above the general noise background, the strongest SST signatures are all very localized to narrow straits and sills where semidiurnal tidal currents are very large. Many of these straits are also where the main Indonesian throughflow occurs, so the mixing marked by these strong SST anomalies surely reflects the tidal mixing that has long been recognized to occur as part of the throughflow. The surprise, at least relative to some previous depictions, is that the mixing is so localized. But there have been earlier intimations that that must be the case [e.g., *Ffield and Robertson*, 2005; *Nagai and Hibiya*, 2015; *Koch-Larrouy et al.*, 2015].

It appears that these ultrahigh resolution SST data could be of great utility in mapping out connections between barotropic-to-baroclinic tidal conversion and locations of greatest tidal mixing. Such efforts should be invaluable in attempts to devise better mixing parameterizations for general circulation models [e.g., *Koch-Larrouy et al.*, 2007; *Nagai and Hibiya*, 2015]. On the other hand, as noted above, it is surely possible that tidal mixing can occur without a spring-neap modulation near the surface. It would then fail to be detected in a tidal analysis for MSf. Modeling or in situ data would be required to recognize such cases. Nonetheless, when an MSf signal in SST does occur, at its distinctive frequency, one can be certain that tides are involved.

We close with a few points regarding the logistics of using SST as a signpost for mixing. Since the SST mixing signatures are so localized, at least in this region of the Indonesian seas, it becomes clear in retrospect that it

is the high-resolution IR data within the MUR-SST product that must be providing the resolution needed for this analysis. In particular, nearly all the small channels and straits displaying high amplitude in Figure 1 must rely on IR data because of the necessary land masking of microwave data. If the mixing signatures were more broad scale and regional, such as first suggested by FG96 when it appeared that most of the whole Banda Sea was involved, then the coarser resolution microwave data would be invaluable since those data are less affected by cloud and aerosol issues.

It thus becomes clear, again in retrospect, that the best approach to extracting tidal mixing signatures from SST data in this region is probably to rely only on high-resolution IR data. Moreover, the IR measurements should then be tidally analyzed at their original temporal sampling. A level 4 product that has interpolated the data onto a fixed temporal sampling is likely to corrupt a near-fortnightly tidal signal if many cloud-induced data gaps have been interpolated across. Equispacing in time is certainly useful for spectral calculations (as in Figure 2), but it is not needed for tidal analysis for which a temporally coherent signal is the target. The history of tidal analysis of satellite altimetry proves the utility of analyzing data at the original temporal sampling, even if that sampling badly aliases the signals.

Acknowledgments
We thank Arnold Gordon for fruitful discussions and two reviewers for useful comments. This work was supported by the Physical Oceanography program of the U.S. National Aeronautics and Space Administration. The Group for High-Resolution Sea Surface Temperature (GHRSST) Multiscale Ultrahigh Resolution (MUR) SST data were obtained from the NASA EOSDIS Physical Oceanography Distributed Active Archive Center at the Jet Propulsion Laboratory, Pasadena, CA.

References

Aiki, H., J. Matthews, and K. Lamb (2011), Modeling and energetics of tidally generated wave trains in the Lombok Strait: Impact of the Indonesian throughflow, *J. Geophys. Res.*, *116*, C03023, doi:10.1029/2010JC006589.

Alford, M. H., M. C. Gregg, and M. Ilyas (1999), Diapycnal mixing in the Banda Sea: Results of the first microstructure measurements in the Indonesian throughflow, *Geophys. Res. Lett.*, *26*, 2741–2744.

Apel, J. R., J. R. Holbrook, A. K. Liu, and J. J. Tsai (1985), The Sulu Sea soliton experiment, *J. Phys. Oceanogr.*, *15*, 1625–1651.

Bisagni, J. J., and M. H. Sano (1993), Satellite observations of sea surface temperature variability on southern Georges Bank, *Cont. Shelf Res.*, *13*, 1045–1064.

Chelton, D. B., and F. J. Wentz (2005), Global microwave satellite observations of sea surface temperature for numerical weather prediction and climate research, *Bull. Am. Meteorol. Soc.*, *86*(8), 1097–1115.

Chin, T. M., R. F. Milliff, and W. G. Large (1998), Basin-scale, high-wavenumber sea surface wind fields from a multiresolution analysis of scatterometer data, *J. Atmos. Oceanic Tech.*, *15*, 741–763.

Chin, T. M., J. Vazquez, and E. Armstrong (2013), *Algorithm Theoretical Basis Document: A Multi-Scale, High-Resolution Analysis of Global Sea Surface Temperature, vers. 1.3*, Jet Propulsion Laboratory, Pasadena.

Donlon, C. J., et al. (2009), The GODAE high-resolution sea surface temperature pilot project, *Oceanography*, *22*, 34–45.

Donlon, C. J., et al. (2007), The Global Ocean Data Assimilation Experiment high-resolution sea surface temperature pilot project, *Bull. Am. Meteorol. Soc.*, *88*(8), 1197–1213.

Doodson, A. T., and H. D. Warburg (1941), *Admiralty Manual of Tides*, HMSO, London.

Egbert, G. D., and S. Y. Erofeeva (2002), Efficient inverse modeling of barotropic ocean tides, *J. Atmos. Oceanic Technol.*, *19*, 183–204.

Ffield, A., and A. L. Gordon (1996), Tidal mixing signatures in the Indonesian seas, *J. Phys. Oceanogr.*, *26*, 1924–1937.

Ffield, A., and R. Robertson (2005), Indonesian seas finestructure variability, *Oceanography*, *18*, 108–111.

Garrett, C. (1979), Mixing in the ocean interior, *Dyn. Atmos. Oceans*, *3*, 239–265.

Hatayama, T. (2004), Transformation of the Indonesian throughflow water by vertical mixing and its relation to tidally generated internal waves, *J. Oceanogr.*, *60*(3), 569–585.

JPL MUR MEaSUREs Project (2010), *GHRSST Level-4 MUR Global Foundation Sea Surface Temperature Analysis, Ver. 1*. PO.DAAC, CA, USA. [Available at http://dx.doi.org/10.5067/GHNMR-4FJ01.]

Koch-Larrouy, A., G. Madec, P. Bouruet-Aubertot, T. Gerkema, L. Bessières, and R. Molcard (2007), On the transformation of Pacific water into Indonesian throughflow water by internal tidal mixing, *Geophys. Res. Lett.*, *34*, L04604, doi:10.1029/2006GL028405.

Koch-Larrouy, A., M. Lengaigne, P. Terray, G. Madec, and S. Masson (2010), Tidal mixing in the Indonesian seas and its effect on the tropical climate system, *Clim. Dyn.*, *34*, 891–904, doi:10.1007/s00382-009-0642-4.

Koch-Larrouy, A., A. Atmadipoera, P. van Beek, G. Madec, J. Aucan, F. Lyard, J. Grelet, and M. Souhaut (2015), Estimates of tidal mixing in the Indonesian archipelago from multidisciplinary INDOMIX in-situ data, *Deep-Sea Res.*, *106*, 136–153.

Martínez Díaz de León, A., R. Castro, E. Santamaría del Ángel, I. Pacheco Ruiz, and R. Blanco Betancourt (2013), Sea surface heat fluxes and fortnightly modulation of the surface temperature within the Ballenas Channel, Gulf of California, *J. Coastal Res.*, *29*(6), 1400–1412.

Matthews, J. P., H. Aiki, S. Masuda, T. Awaji, and Y. Ishikawa (2011), Monsoon regulation of Lombok Strait internal waves, *J. Geophys. Res.*, *116*, C05007, doi:10.1029/2010JC006403.

Murray, S. P., and D. Arief (1988), Throughflow into the Indian Ocean through the Lombok Strait, January 1985–January 1986, *Nature*, *333*, 444–447.

Nagai, T., and T. Hibiya (2015), Internal tides and associated vertical mixing in the Indonesian Archipelago, *J. Geophys. Res.*, *120*, 3373–3390, doi:10.1002/2014JC010592.

Osafune, S., and I. Yasuda (2006), Bidecadal variability in the intermediate waters of the northwestern subarctic Pacific and the Okhotsk Sea in relation to the 18.6-year period nodal tidal cycle, *J. Geophys. Res.*, *111*, C05007, doi:10.1029/2005JC003277.

Osborn, T. R. (1980), Estimates of the local rate of vertical diffusion from dissipation measurements, *J. Phys. Oceanogr.*, *10*, 83–89.

Paden, C. A., M. R. Abbott, and C. D. Winant (1991), Tidal and atmospheric forcing of the upper ocean in the Gulf of California: 1. Sea surface temperature variability, *J. Geophys. Res.*, *96*, 18,337–18,359.

Pugh, D., and P. Woodworth (2014), *Sea Level Science: Understanding Tides, Surges, Tsunamis and Mean Sea-Level Changes*, Cambridge Univ. Press, Cambridge.

Ray, R. D. (2007), Decadal climate variability: Is there a tidal connection?, *J. Clim.*, *20*, 3542–3560.

Ray, R. D., G. D. Egbert, and S. Y. Erofeeva (2005), A brief overview of tides in the Indonesian seas, *Oceanography*, *18*, 74–79.

Reynolds, R. W., and D. B. Chelton (2010), Comparisons of daily sea surface temperature analyses for 2007–08, *J. Clim.*, *23*(13), 3545–3562.

Reynolds, R. W., and D. C. Marsico (1993), An improved real-time global sea surface temperature analysis, *J. Clim.*, *6*(1), 114–119.

Rogachev, K. A., E. C. Carmack, A. S. Salomatin, and M. G. Alexanina (2001), Lunar fortnightly modulation of tidal mixing near Kashevarov Bank, Sea of Okhotsk, and its impact on biota and sea ice, *Prog. Oceanogr.*, *49*, 373–390.

Souza, A. J., and J. Pineda (2001), Tidal mixing modulation of sea-surface temperature and diatom abundance in Southern California, *Cont. Shelf Res.*, *21*, 651–666.

Sprintall, J., J. T. Potemra, S. L. Hautala, N. A. Bray, and W. W. Pandoe (2003), Temperature and salinity variability in the exit passages of the Indonesian throughflow, *Deep-Sea Res. II*, *50*, 2183–2204.

Sprintall, J., A. L. Gordon, A. Koch-Larrouy, T. Lee, J. T. Potemra, K. Pujiana, and S. Wijffels (2014), The Indonesian seas and their role in the coupled ocean-climate system, *Nature Geosci.*, *7*, 487–492.

Susanto, R. D., L. Mitnik, and Q. Zheng (2005), Ocean internal waves observed in the Lombok Strait, *Oceanography*, *18*(4), 80–87.

Tessler, Z. D., A. L. Gordon, and C. R. Jackson (2012), Early stage soliton observations in the Sulu Sea, *J. Phys. Oceanogr.*, *42*(8), 1327–1336.

Wentz, F. J., C. Gentemann, D. Smith, and D. Chelton (2000), Satellite measurements of sea surface temperature through clouds, *Science*, *288*, 847–850.